Chapter 6

Pyrolysis of torrefied biomass: Optimization of process parameters using response surface methodology, characterization, and comparison of properties of pyrolysis oil from raw biomass

General background

This chapter aimed to investigate the pyrolysis of torrefied *Acacia nilotica* (TAN-252-60-5) obtained during optimization of torrefaction process as discussed in Chapter 5. Considering pyrolysis oil as the desired product from pyrolysis process, the process parameters such as temperature (400-600 ℃), retention time (30-90 min), heating rate (15-40 ℃/min), and sweeping gas flow rate (40-80 mL/min) were optimized using response surface methodology for maximum pyrolysis oil yield. The raw *Acacia nilotica* (DAN) was also pyrolysed at obtained optimum condition for comparing the physicochemical characteristics of pyrolysis oil from DAN and TAN-252-60-5. The pyrolysis oil obtained from pyrolysis of TAN-252-60-5 (coded as PO-TAN) and from pyrolysis of DAN (coded as PO-DAN) were subjected to FTIR, GC-MS, and ^{13}C NMR analyses along with estimation of water content, pH, viscosity, HHV, etc., for comparing the physicochemical characteristics. In addition, characteristics of pyrolytic gases and biochar obtained at optimum condition form pyrolysis DAN and TAN-252-60-5 were also compared.

6.1 Introduction

The thermochemical processes, for example, combustion, pyrolysis, torrefaction, and gasification, have gained attraction to convert biomass into biofuels due to higher yield of product, lower operational cost, speed of reaction and higher efficiency (Dhanavath et al., 2019). In particular, pyrolysis has gained dominance for conversion of biomass into biochar, pyrolysis oil, and valuable gases (Abas et al., 2018). In pyrolysis process, biomass gets decomposed at elevated temperature in an inert atmosphere (Dai et al., 2019). Pyrolysis oil has been considered as most valuable product from pyrolysis (Guedes et al., 2018). The pyrolysis process is driven by many factors, for example, process temperature (T), retention time (RT), heating rate (HR), sweeping gas flow rate (SGF), and particle size, etc. (Dhyani & Bhaskar, 2018). The optimization of these process parameters becomes very important when it comes to efficiency, economy, and scale-up of pyrolysis reactor system (Singh et al., 2019b).

The pyrolysis oil is an intense dark brown-colored liquid that consists of a large number of chemical compounds (Dhyani & Bhaskar, 2018). Currently, pyrolysis oil is receiving enormous interest since it is regarded as a second-generation biofuel (Lazzari et al., 2019) and may be utilized as a fuel in furnaces, boilers, and engines for generation of heat and power (Zhang et al., 2017) or it may be a good source of various chemicals (Dhyani & Bhaskar, 2018). The pyrolysis of different types of raw biomass and optimization of process parameters for maximum yield of pyrolysis oil has been investigated by many researchers, as mentioned in Chapter 2. However, pyrolysis oil obtained from raw biomass has some drawbacks, for example, high water content, poor volatility, higher acidic value, low heating value, chemical instability, and undesired aging problem (Ro et al., 2018;

Zhang et al., 2017). These characteristics of pyrolysis oil hampered its direct and efficient utilization as fuel (Zhang et al., 2017). Thus, it cannot compete with conventional fuels such as gasoline and diesel. So, there is an urgent demand for upgrading of pyrolysis oil. Various efforts have been made in this field such as catalytic pyrolysis and pretreatment of biomass by torrefaction (Singh et al., 2019b), hydrothermal liquefaction (Nazari et al., 2017) prior to pyrolysis.

The base of the torrefaction is to optimize the operating condition, which can yield improved quality torrefied biomass. However, pyrolysis of that improved torrefied biomass (having maximum HHV and energy yield simultaneously) gained at optimum condition of torrefaction has not been investigated. Less attention has been given towards HHV and energy yield of torrefied biomass. The HHV and energy yield of torrefied biomass are very crucial parameters for energy utilization and densification (Singh et al., 2019b) and play a vital role in deciding quality and quantity of pyrolysis oil obtained from pyrolysis of torrefied biomass. Both these parameters display opposite trend during torrefaction process. The HHV of torrefied biomass increased, while energy yield decreased with temperature. Thus, considering these two parameters, torrefaction process has to be optimized for maximum HHV and energy yield of torrefied biomass. In our previous work (Chapter 6) we have optimized the torrefaction process for maximum HHV and energy yield (Singh et al., 2019b). The optimum condition was attained at 252 ℃, retention time of 60 min, and heating rate of 5 ℃/min. Therefore, in this Chapter, two-stage optimization (optimization of torrefaction process (Stage-1), optimization of pyrolysis process (Stage-2)) of integrated torrefaction-pyrolysis process has been reported.

6.2 Experimental segment

6.2.1 Sample preparation

Torrefied *Acacia nilotica* at optimum torrefaction condition of 252 ℃, 60 min retention time, and 5 ℃/min heating rate (TAN-252-60-5) has been considered as a feedstock for pyrolysis process. Multiple runs of DAN were performed at optimum torrefaction condition for collection of TAN-252-60-5. The detailed discussion about collection, preparation, physicochemical characteristics of DAN has been discussed in Chapter 3.

6.2.2 Design of experimental condition using RSM

To increase the pyrolysis oil yield, it is imperative to know the behavior of each parameter towards the pyrolysis process. This can be done by optimization of process parameters affecting the pyrolysis process. RSM has been considered as one of the most promising and prevalent techniques used for the optimization of process. A three-level, four-factor CCD technique was employed to optimize the independent process variables. The CCD technique was used since it requires minimum set of experimental runs to establish a correlation among independent variables and desired response. Temperature (A), RT (B), HR (C) and SGF (D) in the range of 400-600 ℃, 30-90 min, 15-40 ℃/min and 40-80 mL/min, respectively, were considered as independent process parameters and pyrolysis oil yield was considered as the desired response that needs to be maximized. Table 6.1 represents the coded values of independent process variables. CCD technique consists of axial points (2k), factorial points (2^k), and replicates center points (n_k). The number of experimental runs to be carried out was calculated according to Eq. (6.1):

$$N = 2^k + 2k + n_k = 2^4 + 2(4) + 6 = 30 \quad (6.1)$$

where N signifies number of experimental runs to be carried out, k signifies selected independent variables, and n_k signifies number of replicate central points.

Table 6.1 Coded levels of experimental variables used in CCD method

Independent process variable	Coded experimental levels		
	−1	0	+1
Temperature (℃): A	400	500	600
Retention time (min): B	30	60	90
Heating rate (℃/min): C	15	27.5	40
Sweeping gas flow rate (mL/min): D	40	60	80

The matrix for different experimental conditions is presented in Table 6.2. As per the design matrix, total of 30 experiments were carried out. The yield of pyrolysis oil as the response was correlated with selected independent variables. Few fundamental steps have to be followed during optimization of process variables. First one is to develop a general mathematical relationship among process response and independent variables, given as:

$$Y = f(X_1, X_2, X_3,\ldots\ldots, X_n) \quad (6.2)$$

where Y signifies the desired predicted response, *f* signifies the mathematical relation between desired predicted response and independent process variables, and X_1, X_2,

X_3,…….. X_n signifies n number of independent process variables affecting the desired predicted outcome.

The second step is related to finding the coefficients of developed mathematical co-relation. In CCD technique, usually, a quadratic polynomial equation is suggested for predicting the response. The general quadratic polynomial model of the response can be presented as follows:

$$Y = \beta_0 + \sum_{i=1}^{k} \beta_i X_i + \sum_{i=1}^{k} \beta_{ii} X_i^2 + \sum_{i_{i>j}}^{k} \sum_{j}^{k} \beta_{ij} X_i X_j \quad (6.3)$$

where Y signifies the predicted value of the response, β_0, β_i, β_{ii} , and β_{ij} are constant term and coefficient for linear, quadratic, and interaction terms, respectively, in developed model equation. k signifies the number of independent process variables chosen for optimization of process (here k = 4).

Table 6.2 Experimental design matrix, actual and predicted value of responses

Run	Temp (^{o}C)	Retention time (min)	Heating rate (^{o}C/min)	Sweeping gas flow rate (mL/min)	Pyrolysis oil yield (wt %)	
					Actual	Predicted
1	500 (0)*	60 (0)	27.5 (0)	80 (+1)	33.46	32.91
2	500 (0)	60 (0)	27.5 (0)	60 (0)	31.65	31.63
3	600 (+1)	90 (+1)	40 (+1)	80 (+1)	26.38	26.55
4	600 (+1)	30 (−1)	15 (−1)	40 (−1)	23.76	24.23
5	500 (0)	90 (+1)	27.5 (0)	60 (0)	28.35	28.70
6	400 (−1)	90 (+1)	15 (−1)	80 (+1)	21.93	21.95
7	600 (+1)	90 (+1)	15 (−1)	80 (+1)	22.97	22.86
8	400 (−1)	30 (−1)	40 (+1)	40 (−1)	22.67	23.22
9	500 (0)	60 (0)	27.5 (0)	60 (0)	31.77	31.63
10	400 (−1)	90 (+1)	40 (+1)	40 (−1)	23.60	23.73
11	500 (0)	60 (0)	27.5 (0)	60 (0)	30.93	31.63
12	600 (+1)	30 (−1)	40 (+1)	80 (+1)	25.92	26.56

13	400 (−1)	90 (+1)	15 (−1)	40 (−1)	21.67	21.48
14	400 (−1)	30 (−1)	15 (−1)	40 (−1)	23.95	23.37
15	500 (0)	60 (0)	27.5 (0)	60 (0)	31.92	31.63
16	500 (0)	60 (0)	27.5 (0)	60 (0)	31.67	31.63
17	500 (0)	60 (0)	27.5 (0)	60 (0)	31.41	31.63
18	500 (0)	60 (0)	15 (−1)	60 (0)	30.35	30.98
19	600 (+1)	90 (+1)	40 (+1)	40 (−1)	26.10	25.99
20	500 (0)	60 (0)	40 (+1)	60 (0)	33.51	32.75
21	500 (0)	30 (−1)	27.5 (0)	60 (0)	30.14	29.65
22	400 (−1)	60 (0)	27.5 (0)	60 (0)	24.37	24.08
23	600 (+1)	30 (−1)	15 (−1)	80 (+1)	25.81	25.27
24	500 (0)	60 (0)	27.5 (0)	40 (−1)	32.11	32.51
25	400 (−1)	30 (−1)	15 (−1)	80 (+1)	23.06	23.61
26	600 (+1)	90 (+1)	15 (−1)	40 (−1)	21.85	21.60
27	600 (+1)	30 (−1)	40 (+1)	40 (−1)	26.66	26.23
28	600 (+1)	60 (0)	27.5 (0)	60 (0)	25.88	26.04
29	400 (−1)	30 (−1)	40 (+1)	80 (+1)	22.91	22.75
30	400 (−1)	90 (+1)	40 (+1)	80 (+1)	23.52	23.49

*Values in the parenthesis are coded level in response surface methodology

In third step, ANOVA is employed to analyze the result of optimization process. The yield of pyrolysis oil, obtained from experiments was taken as actual values, while, predicted values were obtained from a software package (Stat-Ease Design-Expert version 11, USA). The statistical fitness of developed model was investigated by several variables provided in ANOVA analysis. The dependence of yield of pyrolysis oil on different independent variables was checked by p and F values. In addition, various determination coefficients such as R^2, R^2_{pred}, and R^2_{adj}, as well as degree of freedom, were also analyzed to authenticate the reliability of the developed model. Further, the impact of individual and interaction terms of independent process variables on pyrolysis oil yield was examined by 3D surface and contour plots.

6.2.3 Experimental process for pyrolysis

The detailed about the experimental setup and procedure for torrefaction has been mentioned in Chapter 3. In this study, similar procedure was followed during pyrolysis. The pyrolysis of TAN-252-60-5 was carried out between 400-600 ℃ with RT 30-90 min, HR 15-40 ℃/min, and SGF 40-80 mL/min as per the experimental design matrix presented in Table 6.2. During each pyrolysis experiment, 4 g of TAN-252-60-5 was used. Every experiment under similar operating conditions was repeated twice for validation of results. The yield of pyrolysis oil, biochar and pyrolytic gases were obtained by using Eq. (6.4)-(6.6):

$$\text{Pyrolysis oil yield (wt \%)} = \frac{\text{Wt. of bio-oil(g)}}{\text{Wt. of TAN-252-60-5 (g)}} \times 100 \quad (6.4)$$

$$\text{Biochar yield (wt \%)} = \frac{\text{Wt. of biochar(g)}}{\text{Wt. of TAN-252-60-5 (g)}} \times 100 \quad (6.5)$$

$$\text{Pyrolytic gas yield (wt \%)} = 100 - (\text{Pyrolysis oil yield} + \text{Biochar yield}) \quad (6.6)$$

Now, considering upgraded pyrolysis oil as desired product from pyrolysis of TAN-252-60-5, the energy yield and energy conversion efficiency can be obtained by using Eq. (6.7) and Eq. (6.8), respectively.

$$\text{Energy yield of pyrolysis oil} = \text{mass yield} \times \frac{HHV\ of\ pyrolysis\ oil}{HHV\ raw\ Acacia\ nilotica} \quad (6.7)$$

$$\text{Energy conversion efficiency} = \frac{Energy\ output}{Energy\ input} \times 100 \quad (6.8)$$

where energy input and energy output can be calculated by using Eq. (6.9) and Eq. (6.10), respectively.

$$\text{Energy input} = \text{weight of DAN} \times \text{HHV of DAN} \quad (6.9)$$

$$\text{Energy output} = \text{weight of pyrolysis oil} \times \text{HHV of pyrolysis oil} \quad (6.10)$$

6.2.4 Analysis of pyrolysis oil, biochar and pyrolytic gases obtained at optimum condition of pyrolysis

The pyrolysis oil obtained from both the feedstocks at optimum conditions were subjected to estimation of physicochemical characteristics. The HHV of pyrolysis oil and biochar was enumerated using a bomb calorimeter (Model C-200, IKA, Germany). The Ramsbottom Carbon residue (RCR- IP 14/65) method was employed for the estimation of carbon residue of pyrolysis oil. ASTM D1298 protocol was employed to estimate the density of pyrolysis oil. The water content of pyrolysis oil was assessed by applying Karl Fischer titrator (ESICO, μP KARL FISCHER moisture titrator) following ASTM D1744 protocol. The viscosity of pyrolysis oil was measured using Brookfield digital viscometer (LVDV-II+Pro). The chemical characteristics, functional groups, and various classes of chemical compounds present in pyrolysis oil were examined by employing FTIR and GC-MS analyses, respectively. Fourier transform infrared spectroscopy (FTIR, Varian 1000, USA) was used to recognize the characteristic peaks associated with various chemical compounds associated with pyrolysis oil and biochar, while GC-MS (model-Shimadzu QP 2010 plus) was used to determine the relative amount of various class of chemical. Helium was used as a carrier gas with 1.21 mL/min flow rate. 1 μL of PO-DAN and PO-TAN-252-60-5 was injected (injector temperature of 260 ℃) into the column (-RXi-5 Sil MS) having dimension of (30 m X 0.25 mm X 0.25 µm). The split ratio of column was 10:1. The initial temperature of GC oven was kept at 50 ℃ (5 min hold) and then heated to 250 ℃ at a rate of 5 ℃/min (again 5 min hold). Finally, the oven heated to 280 ℃ at a rate of 10 ℃/min for holding time of 5 min. The peaks obtained have been identified by using the National Institute of Standards and Technology library (NIST, USA). ^{13}C nuclear magnetic

resonance spectrometry was used to analyze the various type of carbon, and their distribution in PO-DAN and PO-TAN obtained at optimum condition of pyrolysis. The pyrolysis oil was dissolved in deuterated chloroform ($CDCl_3$), and NMR spectra were recorded by Bruker 500 MHz spectrometer (Magnetic system 500'54 ascend ULH) operating at 5 T with a 5 mm BBO BB-1H probe at room temperature with a relaxation delay of 2 s. The standard protocols ASTM E871 for moisture content, ASTM E1755 for ash content, and ASTM E872 for volatile matter were followed to execute proximate analysis of biochar from DAN and TAN-252-60-5. The fixed carbon of both biochars was obtained by difference. The CHNS analyzer instrument and software (EURO EA3000, EURO VECTOR, Italy) was used to investigate the elemental composition of both biochars. The elemental oxygen was obtained by difference considering insignificant sulfur content. The surface characteristics such as morphology and elements that exist on surface of biochar from pyrolysis of DAN and TAN-252-60-5 were studied by Scanning Electron Microscopy (SEM) and Energy-Dispersive X-ray spectroscopy (EDX) (Model JEOL JSM5410, Japan). The pyrolytic gases were analyzed in gas chromatography (GC-TCD Centurion Scientific, model number-5800, New Delhi). Argon was used as carrier gas. The injector, column, and detector temperature were 80, 60, and 150 ℃, respectively.

6.3 Results and discussion

6.3.1 Statistical analysis of developed model

Fig. 6.1 shows the actual and predicted values of response variable (pyrolysis oil yield), where 45° line represents the predicted yield, and the discrete data points represent experimental yield. It is perceived that both actual and predicted values of response are

very close over a wide range of yield of pyrolysis oil; thus, it may be suggested that the developed model excellently represents pyrolysis data. Also, the correlation coefficient (R^2) value is 0.9758, suggesting that developed relation between independent and dependent variables is highly reliable. The polynomial equation between response (pyrolysis oil yield) and variables (T (A), RT (B), HR (C), and SGF (D)) is given by Eq. (6.11).

$$Y_{\text{pyrolysis oil}}\ (\text{wt \%}) = 31.76 + 0.979A - 0.474B + 0.884C + 0.536AC + 0.599BC - 6.01A^2 - 1.90B^2 \quad (6.11)$$

The statistical fitness of developed model has been investigated by ANOVA. The ANOVA is presented in Table 6.3. The statistical fitness of developed model is also confirmed by p-value, which is < 0.005, and higher F-value of 126.59. The model terms having a p-value < 0.0500 are significant. In present developed model, A, B, C, AC, BC, A^2, B^2 are significant model terms. The discrepancy among predicted R^2 and adjusted R^2 should be $<$ 0.2 for reasonable agreement between two coefficients. In this case, predicted R^2 and adjusted R^2 values were 0.9548 and 0.9681, respectively, showing a good agreement. Adequate precision signifies the signal to noise ratio, and its value should be > 4 for significant model. In the case of present developed model, the value of adequate precision was 30.403 showing that developed model can be used for design and scale-up.

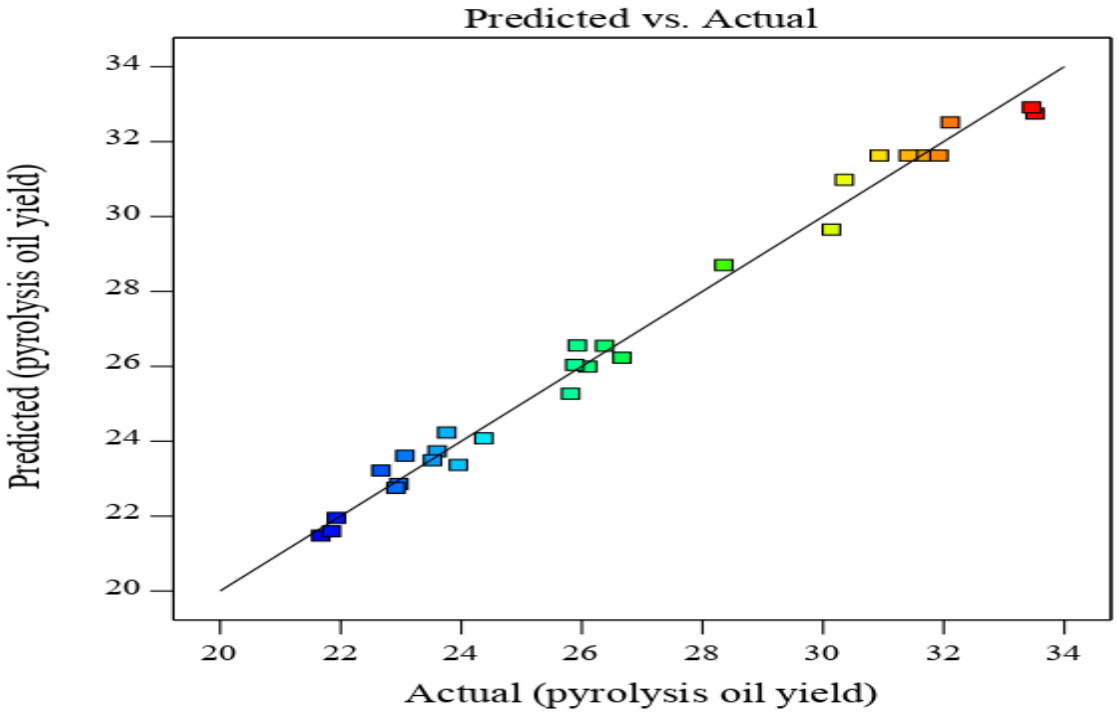

Figure 6.1 Relationship between actual and predicted values of pyrolysis oil

6.3.2 Effect of process variables on yield of pyrolysis oil

6.3.2.1 Individual effect of process parameters

The pyrolysis of biomass was carried out by varying four independent parameters, namely, temperature, heating rate, retention time, and sweeping gas flow rate. The temperature during the pyrolysis supply the required heat for cleavage of bonds associated with biomass (Guedes et al., 2018). As a result, the pyrolysis oil yield increased with increase in temperature, however, after certain temperature, secondary cracking of volatiles dominates, which results in decrease in pyrolysis oil yield and increase in yield of pyrolytic gases

(Guedes et al., 2018). The heating rate during the pyrolysis of biomass significantly affects the yield of pyrolysis oil. In the selected range of heating rate (15-40 ℃/min), the yield of pyrolysis oil increased monotonously with heating rate. Thus, maximum yield of pyrolysis oil was obtained at 40 ℃/min. The higher heating rate during pyrolysis favors the thermal cracking, fragmentation, and depolymerization reaction of biomass, which results in increase in yield of pyrolysis oil (Tripathi et al., 2016). The yield of pyrolysis oil decreased with increase in retention time during pyrolysis of biomass because higher retention time favors cross-linking and repolymerization reaction of biomass, which supports the formation of biochar (Akhtar & Saidina Amin, 2012). The pyrolysis environment also affects the yield of pyrolysis oil. At lower sweeping gas flow rate, the interaction between vapor and solid causes exothermic reaction (Akhtar & Saidina Amin, 2012). As a result, biochar yield increased at lower sweeping gas flow rate. However, at very high sweeping gas flow rate, the condensable vapor might be drained out of the reactor, which may also decrease the yield of pyrolysis oil (Demiral & Şensöz, 2006). Meanwhile, it is important to mention that the effect of individual parameters is also governed by other parameters during pyrolysis process. The interaction of process variables is, therefore, of crucial importance for deciding the yield of pyrolysis oil.

6.3.2.2 Interaction effect of process parameters based on RSM on yield of pyrolysis oil

The effect of process variables (T, RT, HR, and SGF) on the pyrolysis oil yield was examined by 3D surface and contour plots using RSM exported from Design-Expert software. In 3D plots, the impact of two parameters was investigated at one time on

pyrolysis oil yield. The remaining two parameters were kept constant because it is not possible to show the effect of more than two parameters simultaneously on 3D plots (Mohammed et al., 2017c). The significance of individual parameters, their interaction effect with each other, and square of parameters on pyrolysis oil yield was deduced using ANOVA.

Fig. 6.2 (a and b) represent the 3D surface and contour plot for pyrolysis oil yield where the combined influence of temperature and retention time at fixed heating rate (27.5 ℃/min) and sweeping gas flow rate (60 mL/min) was examined. Results displayed that the pyrolysis oil yield increased to a maximum value, then started to decrease as the temperature and retention time continuously increased. An increase in temperature favors the formation of more volatiles; however, after specific temperature, due to secondary cracking reaction, volatiles might be converted into gaseous products such as H_2, CH_4, and CO (Guedes et al., 2018). While, increase in retention time favors the cross-linking and repolymerization reaction, which results in higher bio-char yield (Akhtar & Saidina Amin, 2012). From Table 6.3, it can be observed that temperature (A) is having F-value 33.97 and 244.97 for individual and square terms, respectively, and p-value less than 0.005 for both the terms. For retention time (B), the F-value for individual and square term is 7.96 and 24.35, respectively, and the p-value less was than 0.005 for both the terms. Thus, temperature (A) and retention time (B) individually and their squared terms (A^2, B^2) are significant for maximum yield of pyrolysis oil. However, interaction term (AB) related to temperature and retention time is not significant due to its p-value (0.2049) greater than 0.005. Similarly, the term (AD), which corresponds to the interaction between temperature and sweeping gas flow rate, is not significant because of higher p-value (0.1808). The p-

value of all non-significant terms is not shown in ANOVA table since only significant terms have been considered and mentioned in ANOVA table.

Table 6.3 ANOVA of quadratic model for pyrolysis oil response and corresponding model terms

Source	Sum of square	Degree of freedom	Mean of square	F-value	p-value	Remark
Pyrolysis oil yield						
Model	**450.70**	**7**	**64.39**	**126.59**	**< 0.0001**	Significant
A-Temp	17.28	1	17.28	33.97	< 0.0001	Significant
B-RT	4.05	1	4.05	7.96	0.0100	Significant
C-HR	14.09	1	14.09	27.71	< 0.0001	Significant
AC	4.61	1	4.61	9.07	0.0064	Significant
BC	5.76	1	5.76	11.32	0.0028	Significant
A^2	124.59	1	124.59	244.97	< 0.0001	Significant
B^2	12.38	1	12.38	24.35	< 0.0001	Significant
Residual	4.79	15	0.3191			
Lack of Fit	10.58	17	0.6223	5.10	0.0802	not significant
Pure Error	0.6097	5	0.1219			
Cor Total	461.89	29				
Std. Dev		0.7132		R-Squared		0.9758
Mean		27.01		Adjusted R-Squared		0.9681
C.V		2.64		Predicted R-Squared		0.9548
PRESS		27.24		Adequate Precision		30.407

The coupled impact of temperature and heating rate at fixed retention time and sweeping gas flow rate of 60 min and 60 mL/min, respectively, are displayed in Fig. 6.2 (c and d). The results inferred that pyrolysis oil yield increased with an increase in heating rate, and the maximum yield of pyrolysis oil was attained at the highest value of heating rate. In contrast to temperature, pyrolysis oil yield increased to a maximum value then started to decrease. The thermal cracking and fragmentation of biomass occur with increased heating

rate during pyrolysis, which increases the pyrolysis oil yield (Tripathi et al., 2016). Also, heating rate during pyrolysis significantly affects the depolymerization reaction of biomass, which releases primary volatile components and added to the more liquid condensate (Dhyani & Bhaskar, 2018). Statistically, the individual term related to heating rate (C) and interaction term of heating rate with temperature (AC) is significant since both the terms have a lower p-value than 0.005 (Table 6.3). The F-values for temperature and heating rate are 33.97 and 27.71, respectively. Thus, the temperature influences pyrolysis more markedly than heating rate. However, the squared term related to heating rate (C^2) is not significant due to its higher p-value (0.5103).

Fig. 6.2 (e and f) display the coupled influence of temperature and sweeping gas flow rate at a constant heating rate (27.5 ℃/min) and retention time (60 min). The result shows that the maximum pyrolysis oil yield was obtained at a minimum sweeping gas flow rate in the selected range (40-80 mL/min). At a higher gas flow rate, the vapor formed might be drained out from the condenser. As a result, pyrolysis oil yield decreases, and gaseous yield increases (Guedes et al., 2018). However, at a very low sweeping gas flow rate, retention time of vapor inside the reactor increases, which might result in a secondary cracking reaction of vapor (Tripathi et al., 2016). The statistical analysis confirmed that all the terms (individual, squared, and interaction with temperature) related to the sweeping gas flow rate are not significant for maximum yield of pyrolysis oil because of higher p-value (Table 6.3). The interaction effect of heating rate and retention time is shown in Fig. 6.2 (g and h), while, interaction effect of sweeping gas flow rate and retention time is shown in Fig. 6.2 (i and j). The flat nature of 3D plots indicates that coupled effect of these process variables on the yield of pyrolysis oil is minimal in the selected range of variables. Similar results were

also obtained in case of effect of sweeping gas flow rate and heating rate on pyrolysis oil yield, as shown in Fig. 6.2 (k and l). Thus, based on the F-value obtained from ANOVA, temperature is the most significant parameter followed by heating rate, retention time, and sweeping gas flow rate, respectively, for maximum pyrolysis oil yield.

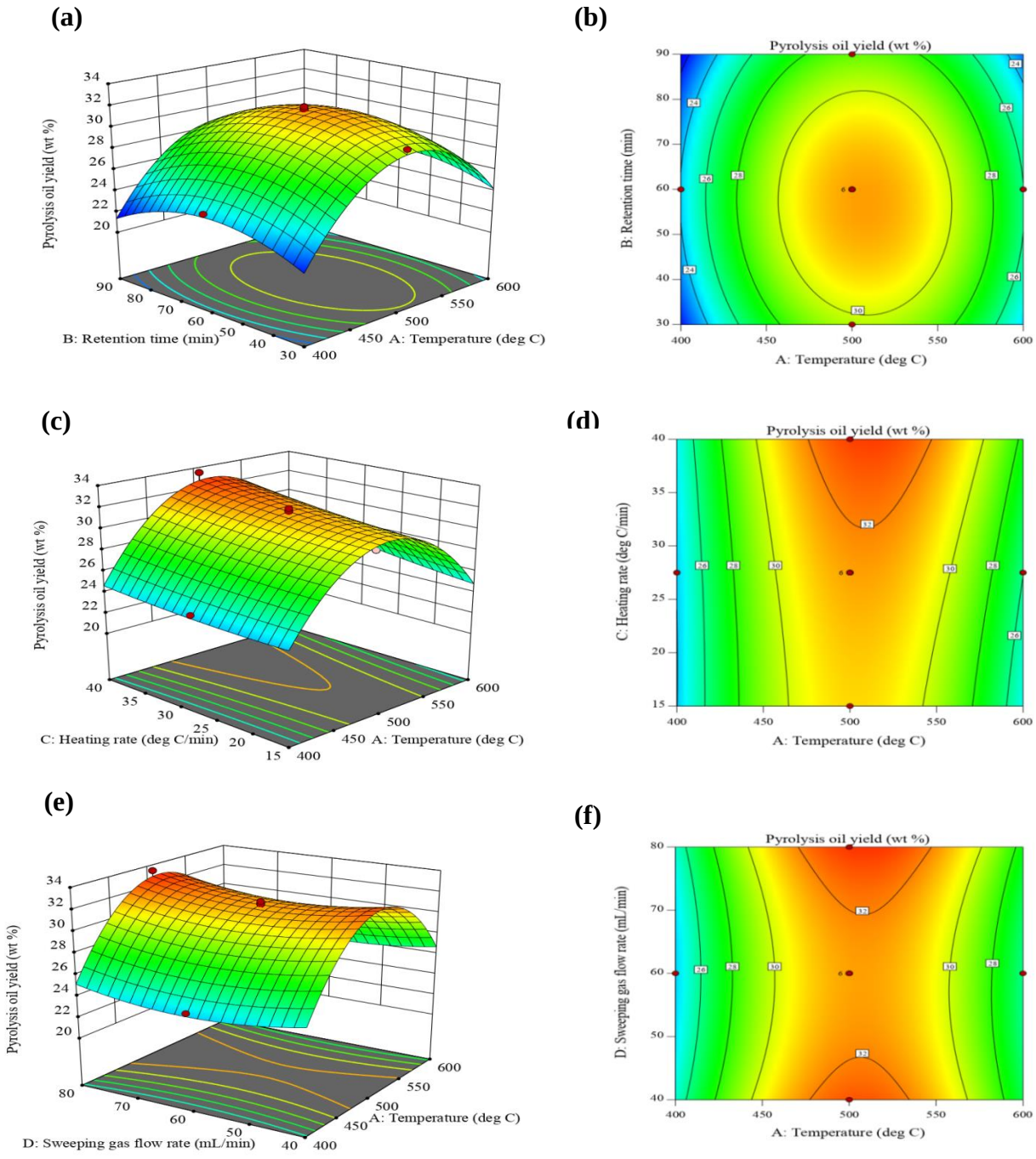

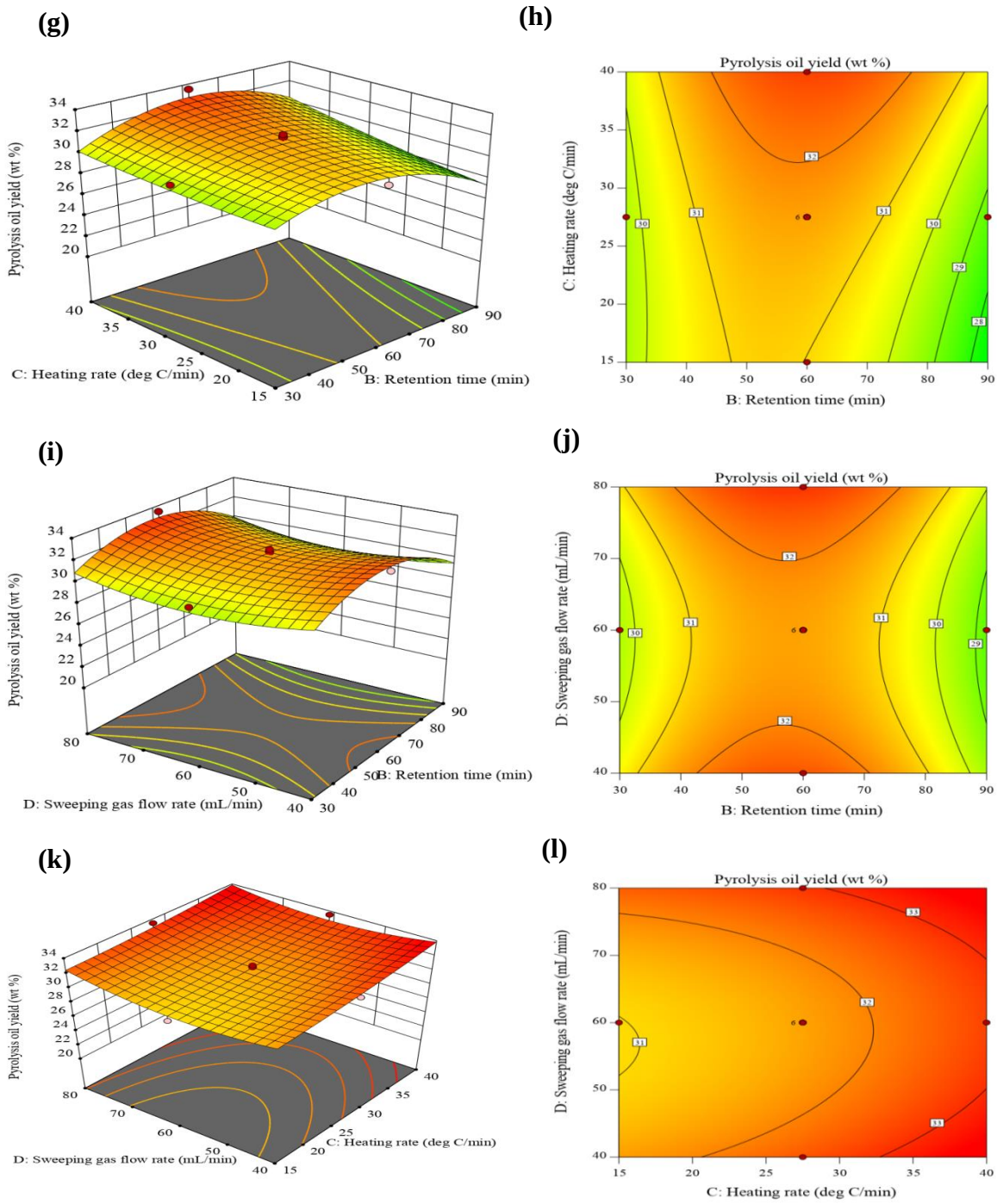

Figure 6.2 Three dimensional response surface and contour plots of pyrolysis oil yield depicting the effect of (a) and (b) temperature and retention time, (c) and (d) temperature and heating rate, (e) and (f) temperature and sweeping gas flow rate, (g) and (h) retention time and heating rate, (i) and (j) retention time and sweeping gas flow rate, (k) and (l) heating rate and sweeping gas flow rate

6.3.3 Validation of process parameters for yield of pyrolysis oil

The optimum condition for the experiment was attained by considering the independent process parameters in experimental range and dependent parameter (pyrolysis oil yield) to be the maximum (Table 6.4). Considering the above conditions, total hundred solutions were provided by the design expert statistical software. However, the solution having the highest desirability was taken into consideration. The optimum values of independent process variables for maximum pyrolysis oil yield (33.56 wt %) were found to be: T of 507.04 ℃, RT of 58.25 min, HR of 38.00 ℃/min, and SGF of 40.53 mL/min. This optimum condition obtained by design expert software was experimentally validated by performing the actual experiments at slightly different conditions (T of 507 ℃, RT of 58 min, HR of 38 ℃/min, and SGF of 40 mL/min) due to instrumental constraints of electric furnace and mass flow controller. The experimental and predicted values are given in Table 6.5. Based on the difference in experimental and predicted value of yield of pyrolysis oil, the error was calculated and mentioned in Table 6.5. The experimental and predicted values for yield of pyrolysis oil were close enough (Error 3.64%) to certify the reliability of developed model. Further, at similar optimum conditions (T of 507 ℃, RT of 58 min, HR of 38 ℃/min, and SGF of 40 mL/min), pyrolysis of DAN was also performed to examine the differences in physicochemical properties of pyrolysis oil from DAN and TAN-252-60-5. During each pyrolysis experiment, 4 g of TAN-252-60-5 and DAN was used. The experiments were carried out in replicate, and average yield of pyrolysis oil was reported. The yield of pyrolysis oil at optimum condition was 34.83 wt % for pyrolysis of TAN-252-60-5, while it was 45.62 wt % for pyrolysis of DAN.

Table 6.4 Independent variables and response as constraints for optimization

Parameters	Objective	Lower limit	Upper limit
Temperature (^{o}C)	In range	400	600
Retention time (min)	In range	30	90
Heating rate (^{o}C/min)	In range	15	40
Sweeping gas flow rate (mL/min)	In range	40	80
pyrolysis oil yield	Maximum	21.67	33.51

Table 6.5 Experimental and predicted values of pyrolysis oil yield at optimum condition

Run	Temp (℃)	RT (min)	HR (℃/min)	SGF (mL/min)	Yield of pyrolysis oil from TAN-252-60-5 (wt %)		Error (%)
					Experimental	Predicted	
1	507	58	38	40	34.58	33.56	2.94
2	507	58	38	40	35.08	33.56	4.33
Average					34.83	33.56	3.64
At similar optimum condition the yield of pyrolysis oil for DAN was 45.62 wt %							

6.3.4 Yield of pyrolysis oil, biochar and pyrolytic gases at optimum condition from pyrolysis of DAN and TAN-252-60-5

Table 6.6 represents the product yield obtained from pyrolysis of DAN and TAN-252-60-5 at optimum condition of pyrolysis of TAN-252-60-5 for maximum pyrolysis oil yield. Results showed that yield of pyrolysis oil was 10.79 wt % lower, while, yield of pyrolytic

gases and biochar was 3.05 and 7.74 wt %, respectively, was higher for TAN-252-60-5 as compared to DAN. These results were in accordance with the published literature (Chen et al., 2016c; Dai et al., 2019; Zheng et al., 2013). The yield of pyrolysis oil is lower due to lower volatile matter of TAN-252-60-5 and decomposition of lighter volatile compounds into CO_2, CO, H_2O, and acetic acid (Boateng & Mullen, 2013b). Also, the higher ash content of TAN-252-60-5 (Singh et al., 2019b) may catalyze the pyrolysis process to decrease the yield of pyrolysis oil by secondary cracking reaction (Yildiz et al., 2015). The solid biochar yield is higher (Boateng & Mullen, 2013b; Singh et al., 2020b) because of higher cross-linking reaction and charring of TAN-252-60-5 during pyrolysis. The energy yield of pyrolysis oil was evaluated by employing Eq. (6.7). The energy yield of pyrolysis oil represents the amount of energy retained in the pyrolysis oil after pyrolysis (Singh et al., 2019b). The energy yield of pyrolysis oil obtained from pyrolysis of DAN and TAN-252-60-5 was found to be 58.42 and 53.15 %, respectively. The lower value of energy yield for pyrolysis oil from TAN-252-60-5 was obtained because of lower pyrolysis oil yield (Chen et al., 2016a). The energy conversion efficiency for pyrolysis oil was evaluated by employing Eq. (6.8) and it was found to be 58.41 and 43.23 % for pyrolysis oil from DAN and TAN-252-60-5, respectively. The lower energy conversion efficiency was noted for pyrolysis of TAN-252-60-5 due to lower yield of pyrolysis oil.

Table 6.6 The average **y**ield of pyrolysis oil, pyrolytic gases and biochar at optimum condition from pyrolysis of DAN and TAN-252-60-5

Yield	Pyrolysis of DAN	Pyrolysis of TAN-252-60-5
Pyrolysis oil (wt %)	45.62	34.83
Pyrolytic gas (wt %)	20.62	23.67
Biochar (wt %)	33.76	41.50

6.3.5 Characteristics of pyrolysis oil obtained at optimum condition of pyrolysis

6.3.5.1 Fourier transform infrared spectroscopy of pyrolysis oil

The FTIR analysis of PO-DAN and PO-TAN obtained at optimum conditions are performed, and their spectra are depicted in Fig. 6.3. The FTIR spectra confirm the existence of various functional groups related to different classes of compounds. The stretching vibration of O-H between 3200-3400 confirms the presence of phenol, alcohol, water; while, vibration of C=O between 1680-1750 cm^{-1} corresponds to aldehyde and ketones (Gupta & Mondal, 2019). The vibration related to C-H stretching and deformation in the waveband of 2855-2926 and 1362-1462 cm^{-1}, respectively, corresponds to presence of alkane in pyrolysis oil (Mandal et al., 2018). The absorption band between 1420- 1610 $cm^{-1}$and 690-900 cm^{-1} ascribes the presence of mono, polycyclic, and substituted aromatic compounds (Isa et al., 2011). Also, for PO-TAN, the intensity of peaks are higher than PO-DAN, indicating the higher amount of aromatic compounds. The reduction of peaks intensity for PO-TAN, between wave number 1100-1260 cm^{-1} attributed to reduction of oxygenated compounds related to alcohol and ether. The FTIR analysis provides a quick technique to identify the class of various chemical compounds (Isa et al., 2011), while gas chromatography-mass spectrometry analysis (GC-MS) can be employed for quantitative analysis of various chemical compounds present in pyrolysis oil.

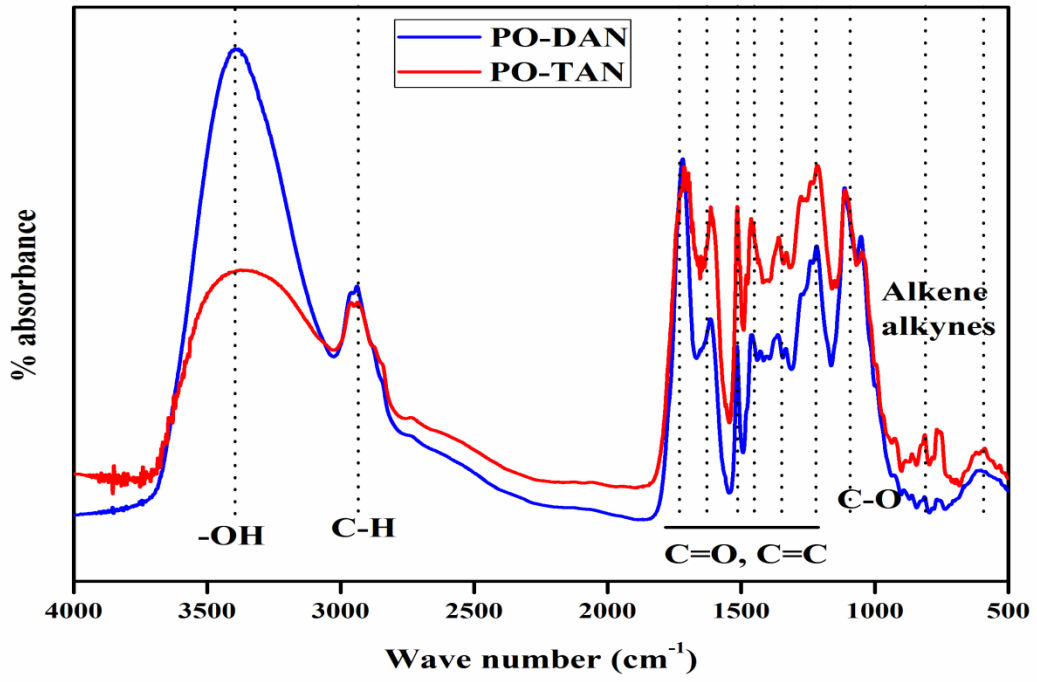

Figure 6.3 FTIR spectra of pyrolysis oil from DAN and TAN-252-60-5 at optimum condition

6.3.5.2 Gas chromatography-mass spectrometry analysis pyrolysis oil

The GC-MS was performed to quantify the various class of chemical compounds exists in PO-DAN and PO-TAN obtained at optimum condition of pyrolysis. The identified chemical compounds are listed in Table 6.7, while GC-MS spectra for PO-DAN and PO-TAN are depicted in Figs. 6.4 (a) and (b). Results showed that PO-DAN and PO-TAN contain various chemical compounds; however, in present study, they were grouped into eight major categories such as acid, aldehydes, ketones, alcohol, esters, phenol derivatives, furan derivatives and sugar derivatives based on their functional groups. It was noted that

quantity of chemical compounds present in both pyrolysis oil varied significantly. Fig. 6.5 depicts the quantitative analysis of various classes of compounds based on the percentage area analyzed by GC-MS analysis. The results showed that PO-TAN contains lower acid, alcohol, and sugar derivatives than PO-DAN. Similar findings were also described by Xin et al. (Xin et al., 2018), Ukaew et al. (Ukaew et al., 2018). This decrease in oxygenated compounds will enhance the stability of pyrolysis oil. It will facilitate the use of pyrolysis oil in bio-refinery at lower cost (Ukaew et al., 2018). Meanwhile, PO-TAN has higher percentage of furan derivatives, phenol derivatives, ketones, and esters than PO-DAN. The decomposition of acetoxy and methoxy groups from hemicellulose results in lower acid content (mainly carboxylic acid) in PO-TAN and ketonization and rearrangement of carboxylic acid results in an increase in ketone content in PO-TAN (Chen et al., 2017). Phenol derivative compounds were mainly formed due to decomposition of lignin present in biomass (Dai et al., 2019).

Table 6.7 Chemical composition of pyrolysis oil identified by GC-MS analysis at optimum condition of pyrolysis of DAN and TAN-252-60-5

Compounds	**Molecular formula**	**Relative content (peak area (%))**	
		PO-TAN	**PO-DAN**
Furan derivatives			
3-Furaldehyde	$C_5H_4O_2$	0.30	0.21
2-Furancarboxaldehyde	$C_5H_4O_2$	10.46	-
2-Furanmethanol	$C_5H_6O_2$	5.62	6.05
Furan, tetrahydro-2,5-dimethoxy-	$C_6H_{13}O_3$	1.04	0.62
2(3H)-Furanone, 5-Methyl-	$C_5H_6O_2$	3.52	5.02
2(5H)-Furanone,5-methyl-	$C_5H_6O_2$	-	0.27
2-Furancarboxaldehyde,-5-Methyl	$C_6H_6O_2$	-	6.45
2-Furanmethanol, Tetrahydro-	$C_5H_{10}O_2$	-	0.44
2-	$C_{16}H_{24}OSi$	-	0.08

Dimethy(trimethylsilylmethyl)silyloxymethyltetrahydrofuran			
Total		**20.94**	**19.14**
Phenol derivatives			
Phenol	C_6H_5OH	3.00	0.97
Phenol, 2-Methyl-	C_7H_8O	-	1.05
Phenol, 2-methoxy-	$C_7H_8O_2$	5.78	
Phenol, 4-methoxy-	$C_7H_8O_2$	-	8.72
Phenol, 2,6-dimethyl-	$C_8H_{10}O$	-	1.25
Creosol	$C_8H_{10}O_2$	3.84	6.05
Phenol, 4-ethyl-2-methoxy-	$C_9H_{12}O_2$	1.62	1.68
2-Methoxy-4-vinylphenol	$C_9H_{10}O_2$	3.79	1.14
Phenol, 2,6-dimethoxy-	$C_8H_{10}O_3$	9.46	9.11
Phenol, 3,4-dimethoxy-	$C_8H_{10}O_3$	-	0.75
3,5-Dimethoxy-4-hydroxytoluene	$C_9H_{12}O_3$	4.63	4.61
Phenol, 2-methoxy-4-(2-propenyl)-	$C_{10}H_{12}O_3$	3.67	0.64
Phenol, 2-methoxy-4-(1-propenyl)-,(E)-	$C_{10}H_{12}O_2$	0.91	-
Phenol, 2,6-dimethoxy-4-(2-propenyl)-	$C_{11}H_{14}O_3$	6.68	0.82
1-Hydroxy-2-methoxy-4-methylbenzene	$C_8H_{10}O_2$	0.37	-
Total		**43.75**	**36.79**
Acids			
dl-3-Methyl-dl-glutamic acid	$C_6H_{11}NO_4$	-	0.54
6-Heptenoic acid, methyl ester	$C_8H_{14}O_2$	-	0.21
Dimethylmalonic acid, dodecyl 3-ethylphenyl ester	$C_{28}H_{56}O_2$	-	0.41
3-Cyclopropenoic acid,-1-butyl, methyl ester	$C_9H_{14}O_2$	-	0.24
2,4-Hexadienedioic acid, 3,4-diethyl-, dimethyl ester, (E,Z)-	$C_8H_{10}O_4$	0.26	-
n-Hexadecanoic acid	$C_{16}H_{32}O_2$	0.60	0.54
Cyclopentanecarboxylic acid	$C_6H_{10}O_2$	0.15	-
Linoelaidic acid	$C_{18}H_{32}O_2$	-	1.90
9-Octadecenoic acid (z)-	$C_{18}H_{34}O_2$	-	0.15
Total		**1.01**	**3.99**
Alcohols			
1-Ethynyl-1-cycloheptanol	$C_8H_{12}O$	-	0.32
1-Penten-3-ol	$C_5H_{10}O$	0.80	0.65
1,2-Benzenediol, 3-methoxy-	$C_7H_8O_3$	0.66	0.28
1,2-Benzenediol, 3-methyl-	$C_7H_8O_2$	-	2.15
1,2,4-Benzenetriol	$C_6H_6O_3$	0.14	-
1-Octen-3-ol, acetate	$C_{10}H_{18}O_2$	0.82	-
3,4-Altrosan	$C_6H_{10}O_5$	0.37	-
trans-Sinapyl alcohol	$C_{11}H_{14}O_4$	0.14	-
Total		**2.93**	**3.40**
Aldehydes			
Benzaldehyde, 4-hydroxy-3-methoxy-	$C_8H_8O_3$	-	0.86
Benzaldehyde, 4-hydroxy-3,5-dimethoxy-	$C_9H_{10}O_4$	0.64	0.64

Coniferyl aldehyde	$C_{10}H_{10}O_3$	0.50	-
trans-Sinapaldehyde	$C_{11}H_{12}O_4$	0.55	-
Total		**1.69**	**1.5**
Ketones			
2-Pentanone, 4-hydroxy-4-methyl-	$C_6H_{12}O_2$	1.45	0.92
3-Penten-2-one, 3,4-dimethyl-	$C_7H_{12}O$	0.42	-
2-Cyclopenten-1-one, 2-methyl-	C_6H_8O	1.15	1.58
Alpha.,.beta.-crotonolactone	$C_4H_4O_2$	2.16	2.16
2-Methyl-3-hexanone	$C_7H_{14}O$	-	0.68
3-Methylcyclopentane-1,2-dione	$C_6H_8O_2$	2.86	3.93
5-Hydroxy-2-heptanone	$C_7H_{14}O_2$	0.30	0.46
Spiro[2.4]heptan-4-one	$C_7H_{10}O$	0.23	-
9-Oxabicyclo[6.1.0]non-6-en-2-one	$C_8H_{10}O_2$	0.14	-
3-Ethylcyclopent-2-en-1-one	$C_7H_{10}O$	-	0.25
4H-pyran-4-one, 3-hydroxy-2-methyl-	$C_6H_6O_3$	-	0.31
Ethanone, 1-(4-hydroxy-3-methoxyphenyl)-	$C_9H_{10}O_3$	0.34	0.25
Ethanone, 1-(4-hydroxy-3,5-dimethoxyphenyl)-	$C_{10}H_{12}O_4$	0.84	0.30
2-Cyclopenten-1-one, 3-ethyl-2-hydroxy-	$C_7H_{10}O_2$	0.54	-
6-Methoxycoumaran-7-ol-3-one	$C_9H_8O_4$	3.61	-
3',5'-Dimethoxyacetophenone	$C_{10}H_{12}O_3$	-	0.41
Total		**14.04**	**11.25**
Sugar derivatives			
1,4:3,6-Dianhydro-.alpha.-d-glucopyranose	$C_6H_8O_4$	0.30	1.47
2,3-Anhydro-d-mannosan	$C_6H_8O_4$	-	0.75
Beta.-D-Glucopyranose, 1,6-anhydro-	$C_6H_{10}O_5$	-	6.39
alpha.-D-Glucopyranose, 4-O-.beta.-D-galactopyranosyl	$C_{12}H_{22}O_{11}$	-	0.42
Total		**0.30**	**9.03**
Esters			
2-(Acetyloxy) Ethyl acetate	$C_7H_{12}O_5$	0.53	
Diethyl Phthalate	$C_{12}H_{14}O_4$	-	0.55
Di-n-octyl phthalate	$C_{24}H_{38}O_4$	0.35	0.31
1,2-Benzenedicarboxylic acid, diethyl ester	$C_{12}H_{14}O_4$	0.51	-
2,4-Hexadienedioic acid, 3,4-diethyl-, dimethyl ester, (E,Z)-	$C_8H_{10}O_4$	0.26+1.24	0.53
Total		**2.89**	**1.53**
Other compounds			
1H-Pyrazole, 3,5-dimethyl-	$C_5H_8N_2$	-	9.34
Bicyclo[2.2.2]octane, 1-fluoro-4-methyl-	$C_9H_{15}F$	-	0.27
Benzene, 1,2,3-trimethoxy-5-methyl-	$C_{10}H_{14}O_3$	3.18	1.91
Butane, 1-chloro-3,3-dimethyl-	$C_6H_{13}Cl$	-	0.32
1,4-Butanediamine, 2,3-dimethoxy-N,N,N',N'-tetramethyl-, [S-(R*,R*)]-	$C_{10}H_{24}N_2O_2$	1.75	-
Total		**4.93**	**11.84**

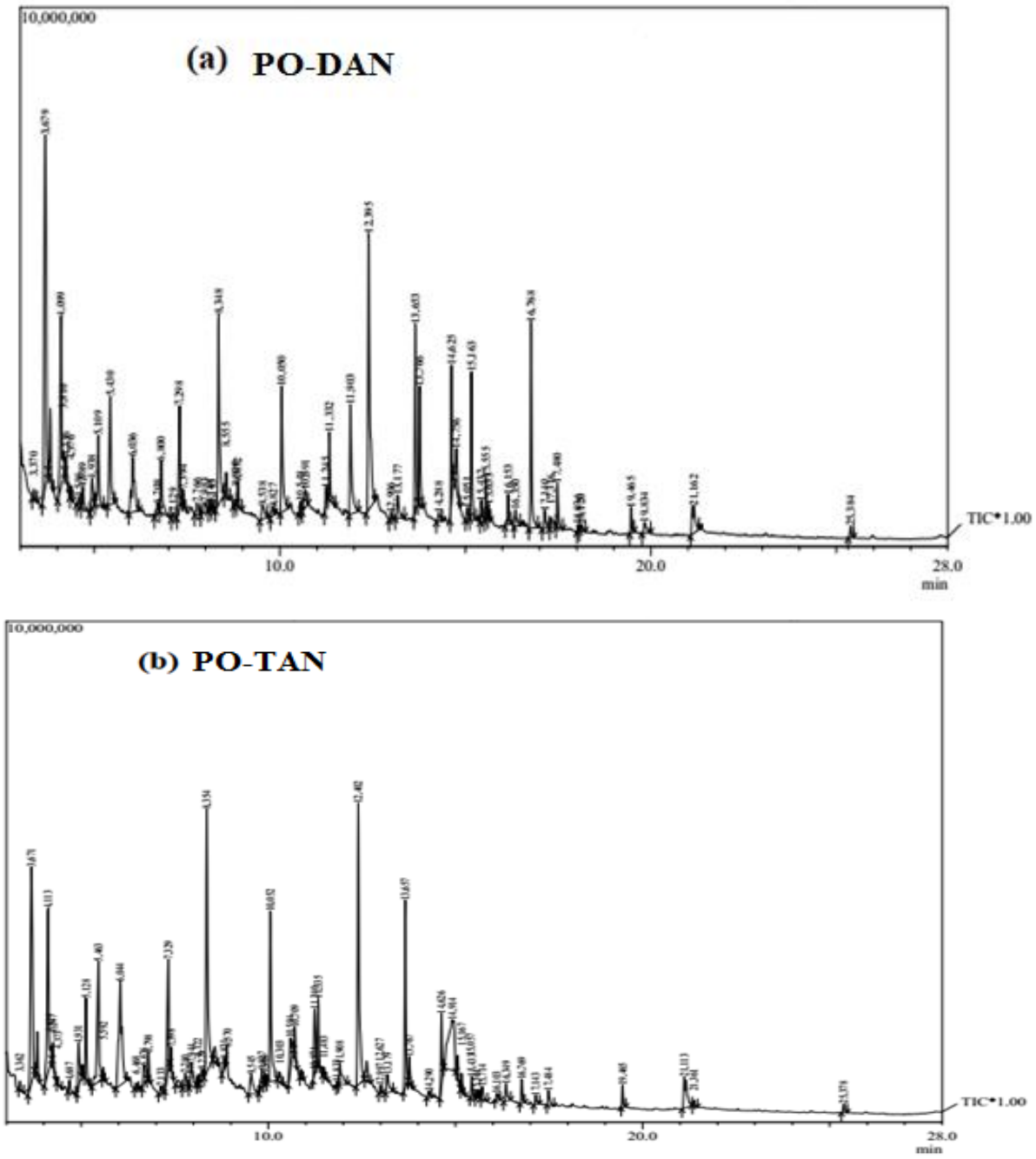

Figure 6.4 GC-MS spectrum of pyrolysis oil from pyrolysis of DAN and TAN-252-60-5 at optimum condition (a) PO-DAN, (b) PO-TAN

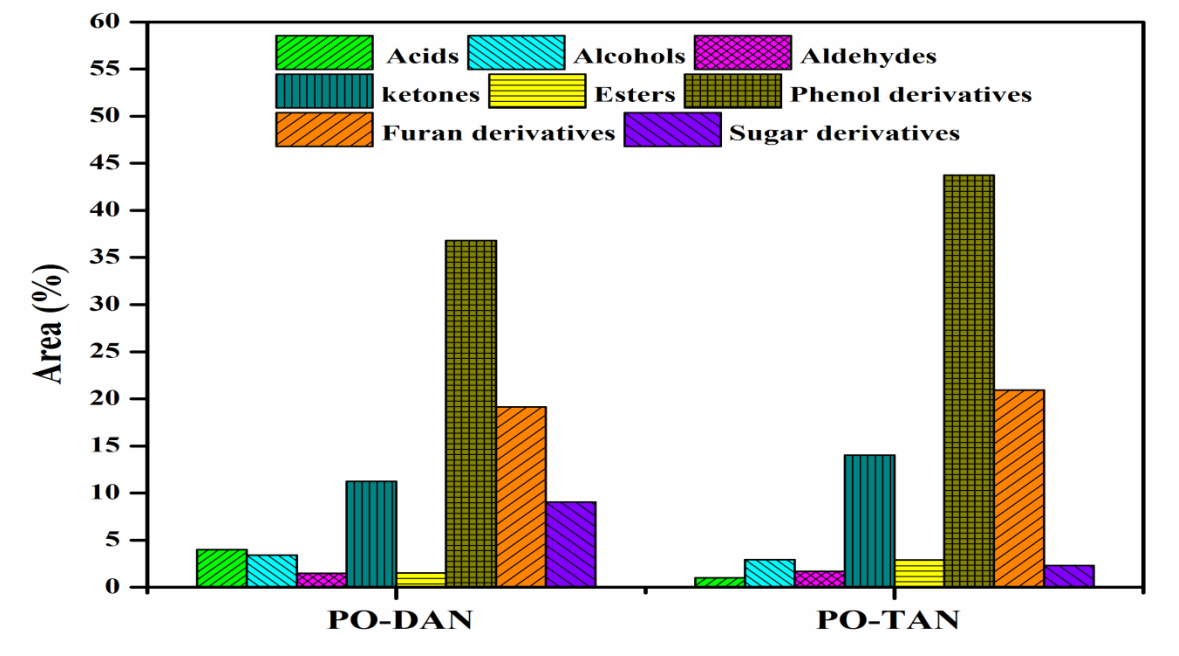

Figure 6.5 The relative amount of different type of compound present in pyrolysis oil from DAN and TAN-252-60-5 obtained at optimum condition

6.3.5.3 ^{13}C NMR analysis of pyrolysis oil

Apart from FTIR analysis, the functional groups and type of carbon present in the pyrolysis oil (PO-DAN and PO-TAN) was also investigated by ^{13}C NMR analysis. The NMR spectra of PO-DAN and PO-TAN are depicted in Fig. 6.6 (a) and (b). The NMR analysis has been considered as a powerful technique to classify the functional groups and type of carbon by dissolving the pyrolysis oil in a suitable solvent and quantify the functional groups by determining the integral area of specific region of spectrum (Negahdar et al., 2016; Xu et al., 2019). The whole NMR spectrum was divided broadly into five chemical shift zones based on the previous work done by Negahdar et al. (Negahdar et al., 2016), Ingram et al. (Ingram et al., 2008), and Joseph et al. (Joseph et al., 2010). The region from 0 to 54 ppm was assigned to alkyl carbon. Also, the alkyl carbon region was sub-divided into primary

alkyl carbon (6-24 ppm) and secondary/tertiary alkyl carbon (24-34 ppm). The chemical shifts from 54 to 70 ppm, 70 to 103 ppm, 103 to 163 ppm, and 163 to 215 ppm were attributed to methoxyl/hydroxyl carbon, carbohydrate carbon, total aromatic carbon, and carbonyl carbon, respectively (Negahdar et al., 2016). Further, the aromatic carbon region was sub-divided into syringyl type carbon (110-112 ppm), guaiacyl type carbon (112-125 ppm). The results related to different types of carbon present in PO-DAN and PO-TAN are presented in Fig. 6.7 (a) and (b), separately. The results showed that total aromatic carbon in PO-DAN and PO-TAN was 24.65 and 34.58 %, respectively. The increase in aromatic carbon in case of PO-TAN may be due to higher lignin content in TAN-252-60-5 than the DAN (Negahdar et al., 2016). The alkyl carbon in PO-DAN and PO-TAN was 36.57 and 28.21 %, respectively. The total alkyl carbon in PO-TAN decreased as compared to PO-DAN. However, primary alkyl carbon in PO-TAN was higher than PO-DAN. This increases the utility of PO-TAN as a fuel. The carbonyl carbon in PO-DAN and PO-TAN was 10.24 and 15.5 %, respectively. The increase in carbonyl carbon may be attributed to an increasing in ketones in case of PO-TAN, as confirmed by GC-MS analysis. A slight decrease in methoxyl/hydroxy carbon was observed in case of PO-TAN (13.16 %) as compared to PO-DAN (15.5 %). This may happen because of decrease in acid content in PO-TAN. The carbohydrate carbon in PO-DAN and PO-TAN was 13.04 and 8.55 %, respectively. The ^{13}C NMR analysis of pyrolysis oil was consistent with the results of GC-MS analysis, as discussed in section 6.3.5.2.

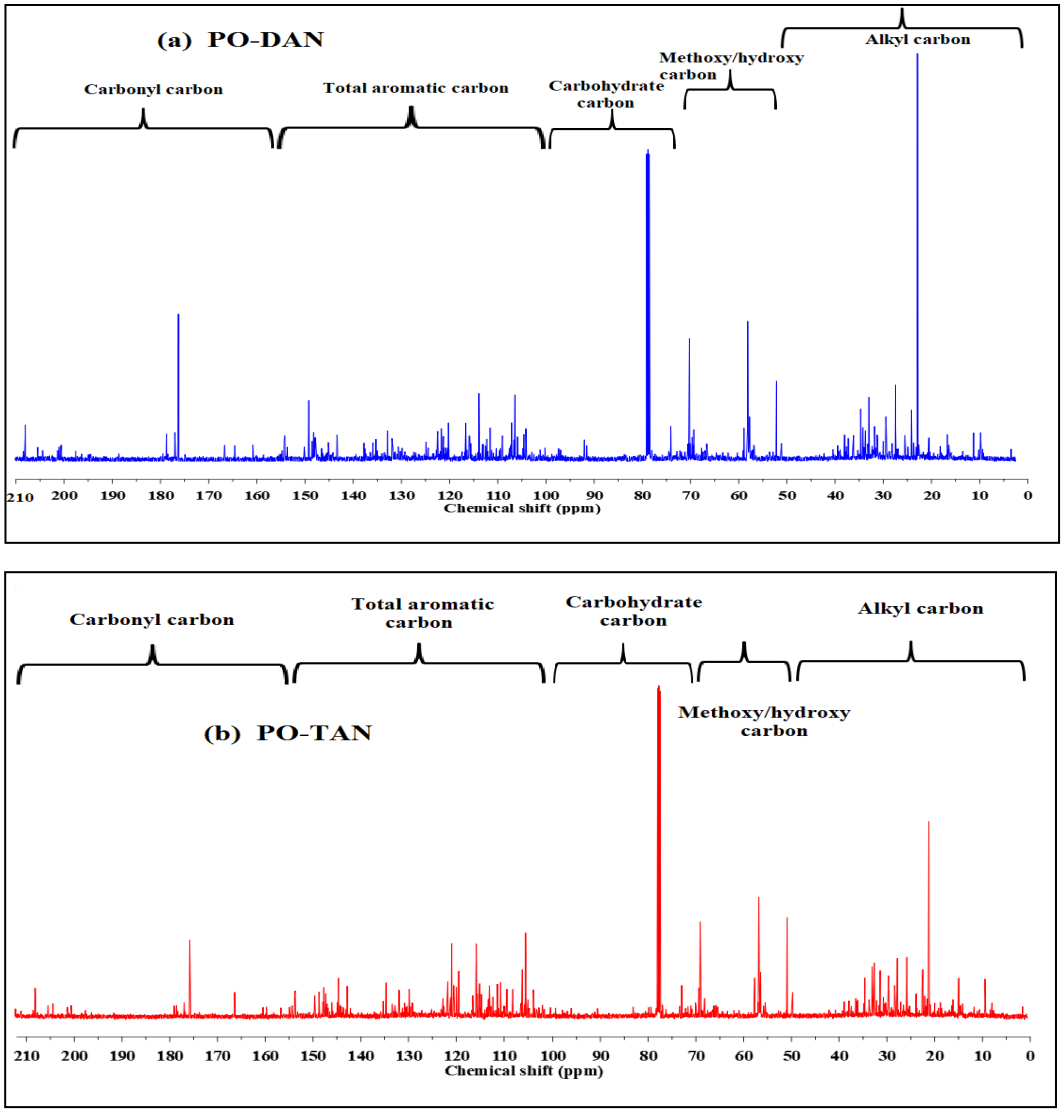

Figure 6.6 ^{13}C NMR spectrum of pyrolysis oil obtained at optimum condition (a) PO-DAN, (b) PO-TAN

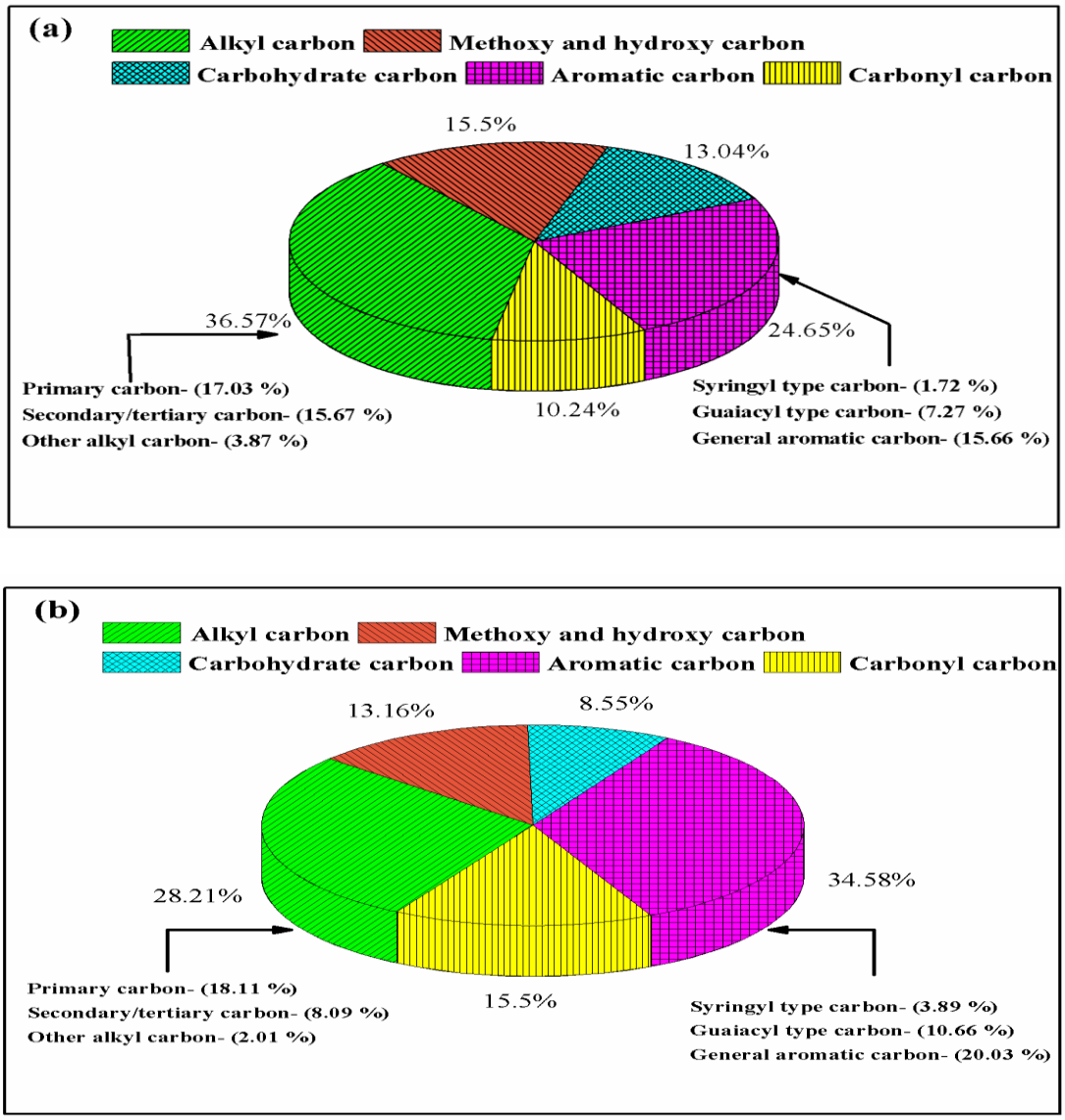

Figure 6.7 The relative amount of different type of carbon present in pyrolysis oil obtained at optimum condition (a) PO-DAN, (b) PO-TAN

6.3.5.4 Physicochemical characteristics of pyrolysis oil

The physicochemical characteristics of pyrolysis oil (PO-DAN and PO-TAN) are mentioned in Table 6.8. The properties of PO-DAN and PO-TAN were compared with standard specification protocol ASTM D7544-12 (ASTM-grade G and ASTM-grade D) (Mohammed et al., 2017c) and physical properties of mineral oils (Dhyani & Bhaskar, 2018). A Minor difference in appearances of PO-TAN and PO-DAN was observed. PO-TAN has an intense dark brownish color with no transparency, while PO-DAN has brownish color having some transparency. The water content of PO-DAN and PO-TAN was found to be 32 and 21 wt %, respectively. The water content in pyrolysis oil is associated with moisture content of native biomass and due to dehydration of pyrolysis products. Lower moisture content in TAN-252-60-5 is attributed to lower water content in PO-TAN. The HHV of PO-DAN and PO-TAN was 24.73 and 30.55 MJ/kg, respectively. The higher HHV of PO-TAN is due to presence of various carbon-rich organic compounds (Mohammed et al., 2017c) and lower water content, which reduces the extra energy consumed in the evaporation of water present in pyrolysis oil. The density of PO-DAN and PO-TAN was 1.098, 1.134 g/cm^3, respectively, while; viscosity was noted to 3.90 and 4.07 cSt, respectively. The lower water content for PO-TAN may be attributed to increasing in density and viscosity. Both the pyrolysis oil (PO-DAN and PO-TAN) show the acidic character having pH value of 2.23 and 3.17, respectively, because of acidic and phenolic compounds present in pyrolysis oil (Mohammed et al., 2017c). However, pH of PO-TAN was 42.15 % higher than the PO-DAN due lower of acidic components. Ramsbottom carbon residue of PO-DAN and PO-TAN was found to be 2.78 and 3.21 wt %, respectively. It depicts the carbon deposition tendency of pyrolysis oil when it is used as a

fuel. The ash content of PO-DAN and PO-TAN was found to be 0.03 and 0.01 wt %, respectively. All physical parameters of PO-DAN and PO-TAN were found in the range of ASTM-grade G and ASTM-grade D. However, PO-TAN has improved properties than PO-DAN. The physical characteristics of both pyrolysis oils vary significantly as compared to mineral oils. This might be due to presence of water and oxygenated compounds present in pyrolysis oil. The higher water and oxygenated compounds attributed to lower heating value and high polarity of pyrolysis oil (Dhyani & Bhaskar, 2018).

Table 6.8 Physicochemical properties of pyrolysis oil (PO-DAN and PO-TAN) at optimum condition and comparison with ASTM grade oil and mineral oils (Dhyani & Bhaskar, 2018; Oasmaa et al., 2009)

Properties	**PO-DAN**	**PO-TAN**	**ASTM-Grade G**	**ASTM-Grade D**	**Heavy fuel oil**	**Light fuel oil**
Appearance	Dark brown	Intense dark brown				
HHV (MJ/kg)	24.73	30.55	Minimum 15	Minimum 15	40.6	42.6
Density (g/cm^3)	1.098	1.134	1.1-1.3	1.1-1.3	0.99-0.995	0.845 (max)
Water content (wt. %)	32	21	Maximum 30	Maximum 30	~0	~0
pH	2.23	3.17	Report	report	-	-
Carbon residue (wt. %)	2.78	3.21	-	-	-	-
Viscosity (cSt)	3.90	4.07	Maximum 125	Maximum 125	180-420	2.0-4.5
Ash content (wt. %)	0.03	0.01	Maximum 0.25	Maximum 0.15	0.08 (max)	0.01 (max)

6.3.6 Characteristics of biochar obtained at optimum condition from pyrolysis of DAN and TAN-252-60-5

6.3.6.1 Proximate and ultimate analyses of biochar

Table 6.9 represents the proximate and ultimate analyses of biochar from pyrolysis of DAN (Biochar-DAN) and TAN-252-60-5 (Biochar-TAN). The moisture content and volatile matter decreased by 29.72 and 31.53 %, while, fixed carbon and ash content increased by 4.58 and 29.58 %, respectively, of Biochar-TAN as compare to Biochar-DAN. The difference in properties of both biochars was associated with the process through which they were obtained. Biochar-DAN was obtained by pyrolysis of DAN, whereas, Biochar-TAN was obtained by thermal treatment of DAN through torrefaction followed by pyrolysis. The intense devolatilization taking place in case of Biochar-TAN results in lesser moisture content and volatile matter and relatively higher fixed carbon and ash content (Dai et al., 2019). Also, in case of Biochar-TAN, the release of hydrogen and oxygen molecules was more prominent than the release of carbon as compared to the Biochar-DAN. The HHV of Biochar-TAN was 10.64 % higher than the Biochar-DAN. The higher HHV of Biochar-TAN was attributed to higher carbon content than Biochar-DAN. The results from proximate and ultimate analysis were similar to the finding of published literature (Chen et al., 2015a; Gogoi et al., 2017).

Table 6.9 Characteristics of biochar obtained at optimum condition from pyrolysis of DAN and TAN-252-60-5

Analysis	Biochar-TAN	Biochar-DAN
Proximate analysis (wt %)		
Moisture content	0.78	1.11
Volatile matter	10.53	15.38
Ash content	8.76	6.97
Fixed carbon*	80.02	76.51
Ultimate analysis (wt %)		
C	86.17	81.38
H	1.01	1.98
N	3.34	2.48
S	BDL	BDL
O*	9.48	14.16
Higher heating value(MJ/kg)	30.55	27.61

*; calculated by difference, BDL; below detection limit

6.3.6.2 SEM-EDX analysis of biochar

Fig. 6.8 (a) and (b) depict the SEM-EDX analysis of Biochar-DAN and Biochar-TAN obtained at optimum condition of pyrolysis. Results showed that surface of both the biochars were heterogeneous, cracked, and having honeycomb-like pore structure (Dhanavath et al., 2019). Biochar-TAN has wide pores as compare to Biochar-DAN because of release of large amounts of volatile matter through intense devolatilization (Dhanavath et al., 2019; Gupta & Mondal, 2019). The pores present on the surface of both biochar may facilitate its potential application in adsorption process (Gupta & Mondal, 2019).

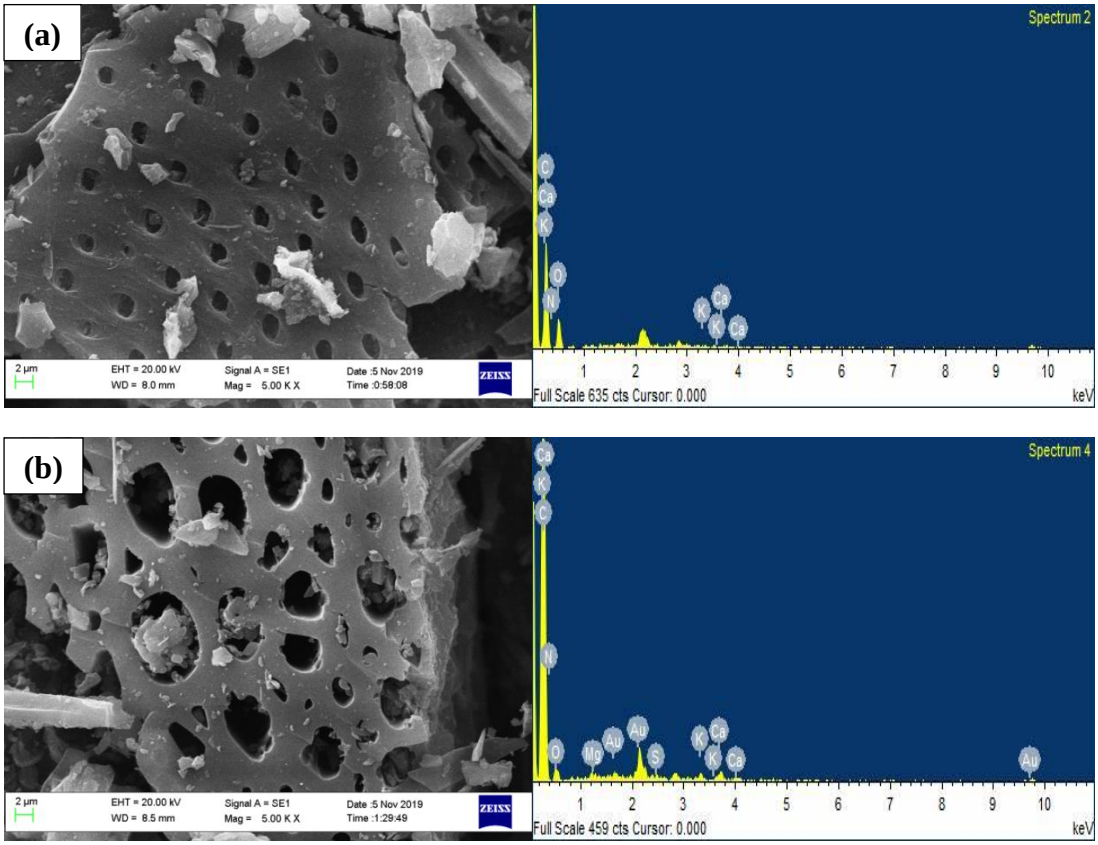

Figure 6.8 SEM-EDX analysis of biochar at optimum condition **(a)** Biochar-DAN **(b)** Biochar-TAN

EDX analysis confirmed that C, K, Ca, O, N existed on the surface of Biochar-DAN, while, C, K, Ca, O, N, Mg existed on the surface of Biochar-TAN. The presence of these macronutrients on the surface of biochar facilitates its utility in soil amendment (Mohammed et al., 2017c). Similar findings were also reported in published literature (Gupta & Mondal, 2019; Mohammed et al., 2017c).

6.3.6.3 FTIR analysis of biochar

The FTIR analysis of Biochar-DAN and Biochar-TAN was performed and their spectra are displayed in Fig. 6.9. The FTIR analysis provides a quick and efficient technique to identify the class of various chemical compounds. The FTIR spectra confirm the presence

of various functional groups associated with biochar. For Biochar-DAN, the peak at 3420.51 cm^{-1} corresponds to stretching vibration of O-H bonded groups such as phenol, alcohol, and water (Gupta & Mondal, 2019). The wavenumber 2925.68 cm^{-1} is ascribed to the stretching and deformation vibration of aliphatic C-H groups. The wavenumber 1688.47 cm^{-1} is assigned to C=O vibration of aldehyde and ketones and C=C aromatic vibrations. The wavenumber 1588.47 cm^{-1} corresponds to secondary amine groups. The wavenumber 1239.84 cm^{-1} is ascribed to deformative vibration of aromatic nitrogen to secondary amine groups. The wavenumber between 876.33- 805.65 cm^{-1} and 757.12-686.51 cm^{-1} ascribe the presence of wagging vibration of C-H bond in aromatic ring and vibration of alkyl halide along with bending vibration of Si-O-Si bond, respectively. Similar results were obtained for Biochar-TAN as well. However, the intensity of peaks for Biochar-TAN was slightly lower than that of Biochar-DAN. This might be due to torrefaction, as considerable rupture of –C-O, -O-H, etc. bonds take place, and there is formation of CO_2 and lighter non-condensable gases (Dai et al., 2019).

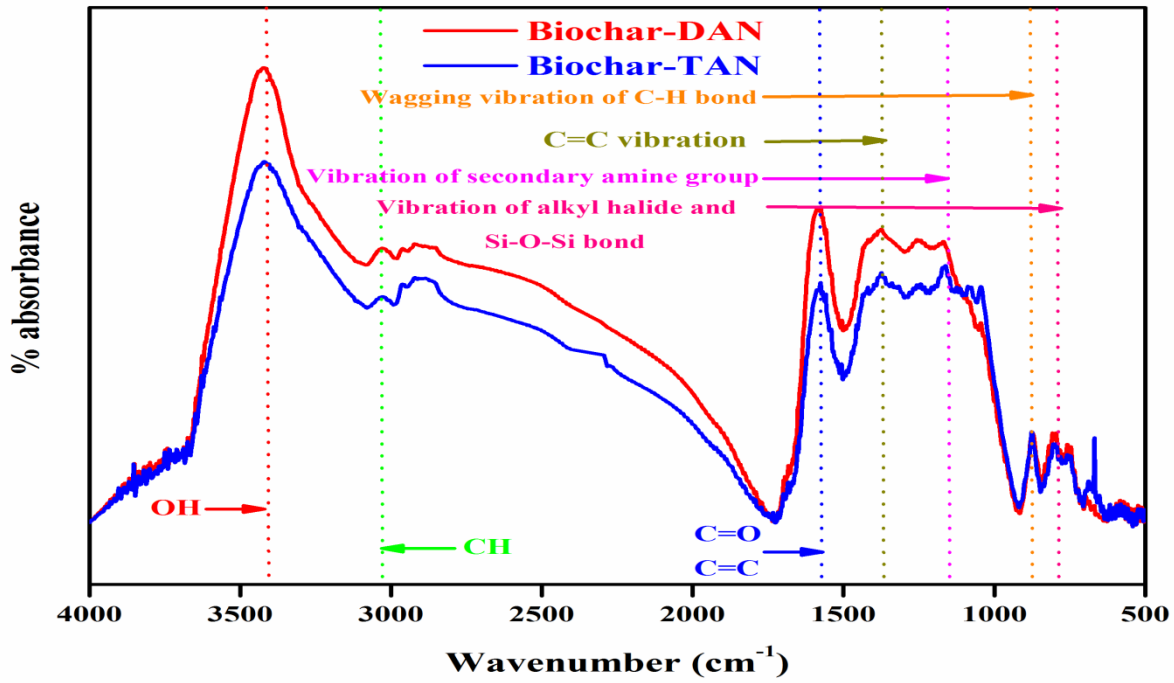

Figure 6.9 FTIR spectra of biochar from DAN and TAN-252-60-5 at optimum condition of pyrolysis

6.3.7 Characteristics of pyrolytic gases obtained at optimum condition from pyrolysis of DAN and TAN-252-60-5

The composition of pyrolytic gases obtained from pyrolysis of DAN and TAN-252-60-5 at optimum condition is displayed in Fig. 6.10. The pyrolytic gases from both the feedstock mainly consist of carbon dioxide (CO_2), carbon monoxide (CO), methane (CH_4) and hydrogen (H_2). Among all gases, the largest amount of CO_2 was present for both the feedstock followed by CO, CH_4, and H_2, respectively. However, significant difference was observed by comparing the composition of pyrolytic gases from DAN and TAN-252-60-5. The mass percentage of CO_2 decreased from 43.05 to 32.71 %, while, mass percentage of

CO, CH_4, and H_2 increased from 32.77 to 35.32, 20.64 to 25.26, 3.54 to 6.70 %, respectively, for pyrolytic gases from TAN-252-60-5 as compared to DAN. CO_2 and CO formed during the pyrolysis as a result of decarboxylation and decorbonylation reactions, respectively (Wang et al., 2018b). Thus, it can be concluded that decarboxylation reaction was more favorable for DAN, while, decarbonylation reaction was more favorable for TAN-252-60-5. The decrease in CO_2 for TAN-252-60-5 pyrolysis was also attributed to degradation of hemicellulose during torrefaction (Konsomboon et al., 2019) The TAN-252-60-5 has higher lignin content as compared to DAN (Singh et al., 2020b). Cleavage of methoxyl group (-OCH_3) through demethoxylation reaction from benzene ring of lignin and presence of large number of alkyl branches in lignin mainly contributed to formation of H_2 and CH_4 (Shen et al., 2010). Small amount of CH_4 was also formed due to breakdown of hemicellulose and cellulose (Yang et al., 2007). The trend of formation of H_2 was in line with CH_4, revealing that generation of H_2 might be complemented by formation of CH_4 (Xin et al., 2013).

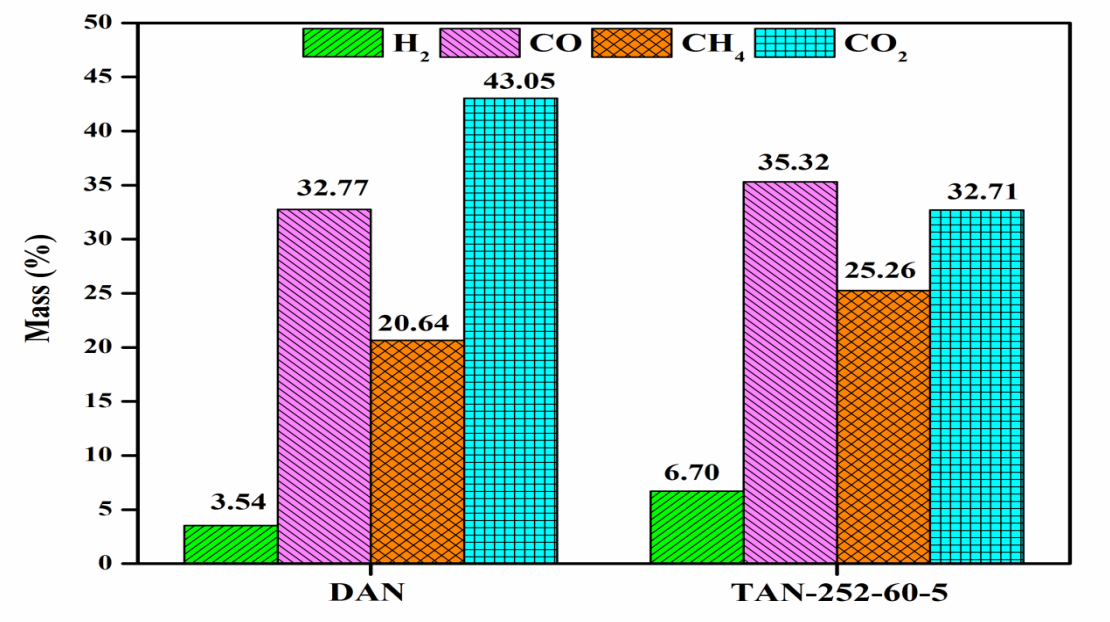

Figure 6.10 Composition of pyrolytic gases from pyrolysis of DAN and TAN-252-60-5 at optimum condition

6.3.8 Mechanism of pyrolysis of TAN-252-60-5

Torrefaction causes physical and chemical modifications in DAN due to which the pyrolysis pathway for TAN-252-60-5 differs from that of DAN because of changes in kinetic parameters, decrease in grinding energy, heat, and mass transfer rate, (Dai et al., 2019). In course of torrefaction, the methenyl groups associated with side chain of hemicellulose are broken, aldose groups detached from main chain of hemicellulose, and all the glycosidic bonds are ruptured; as a result, the hydroxyl bonds of hemicellulose are dehydrated (Dai et al., 2019). The fragmentation of cellulose occurred due to breaking of glycosidic and hydroxyl bonds associated with cellulose (Wang et al., 2017). In addition, slight modification of lignin takes place cleavage of β-O-4 ether bond of benzene ring

associated with lignin (Mahadevan et al., 2016; Wen et al., 2014). The TAN-252-60-5 served better than the DAN since it has lower moisture and oxygen content along with a ruptured surface structure. TAN-252-60-5 has lower activation energy in comparison to DAN (Ren et al., 2013a), which is suggested by loose and porous structure (Singh et al., 2019b). The yield of pyrolysis oil decreases when TAN-252-60-5 is pyrolysed (Boateng & Mullen, 2013b; Chen et al., 2016c), as compared to pyrolysis of DAN; however, there is an enhancement in the characteristics of pyrolysis oil by means of lower water content, oxygenated compounds, and acid content. Also, the amount of total aromatic compounds increases (Chen et al., 2017). The yield of pyrolysis oil is lower due to lower volatile matter of TAN-252-60-5 and decomposition of lighter volatile compounds into CO_2, CO, H_2O, and acetic acid (Boateng & Mullen, 2013b). Also, the higher ash content of TAN-252-60-5 (Singh et al., 2019b) may catalyze the pyrolysis process to decrease the yield of pyrolysis oil by secondary cracking reaction (Yildiz et al., 2015). Also, the pyrolysis of TAN-252-60-5 favors the formation of CH_4 and H_2 as compared to CO_2 and CO (Ren et al., 2013b). The solid biochar yield is higher (Boateng & Mullen, 2013b; Singh et al., 2020b) because of higher cross-linking reaction and charring of TAN-252-60-5 during pyrolysis.

6.3.9 Sustainability of integrated torrefaction-pyrolysis process and implication for cleaner production of pyrolysis oil

Torrefaction was used as a pretreatment step. The desired product was high-quality solid biofuel. However, liquid condensate and gaseous products (CO_2 and CO in large quantity and CH_4 and H_2 in small quantity) are also produced during torrefaction (Chen et al., 2018; Ma et al., 2019). To increase the sustainability of integrated torrefaction-pyrolysis process,

the gaseous products can be used in drying process through combustion of CO, CH_4, and H_2 or may be used to generate heat and electricity for integrated process (Dai et al., 2019). This will reduce the consumption of heat and electricity from external sources. The liquid condensate from torrefaction contains a number of C_1-C_4 oxygenated compounds (Doddapaneni et al., 2017; Liaw et al., 2015) and a large quantity of water (from 40 to 60 wt % depending on the condition of torrefaction) (Chen et al., 2015b; Ma et al., 2019). The liquid condensate may be used to digest CH_4 anaerobically (Doddapaneni et al., 2017; Liaw et al., 2015) or used as a fuel and source of various chemicals after removal of water. Besides, optimization of torrefaction process for high-grade solid biofuel in terms of maximum higher heating value and energy yield can further assist the overall economy, scale-up, and simulation of process by reducing the unnecessary experimental run (Singh et al., 2019b). A general pathway for the sustainability of integrated process is shown in Fig. 6.11.

The pyrolysis oil obtained from pyrolysis of TAN-252-60-5 may have multiple applications, as shown in Fig. 6.12. As mentioned in section 6.3.5.1, the quality of pyrolysis oil obtained from TAN-252-60-5 is superior to pyrolysis oil obtained from DAN in terms of water content, pH value, HHV, etc. In section 6.3.5.3, it is mentioned that oxygen-containing compounds and total acidic compounds in pyrolysis oil from TAN-252-60-5 are lesser as compared to DAN. A pH close to 7 of pyrolysis oil is beneficial as it may reduce the corrosion in fuel system, other equipment, and piping systems during storage and transportation (Dai et al., 2019; Ma et al., 2019). Moreover, decreased water and oxygen-containing compounds may further facilitate upgrading of pyrolysis oil using suitable catalysts because water and oxygen-containing compounds are mainly responsible

for coke formation and deactivation of sites on the surface of a catalysts (Dai et al., 2019). The application of pyrolysis oil has been reported by many authors. For instance, Kurji et al. (Kurji et al., 2016) used the blend of pyrolysis oil for turbine operation. Stamatov et at. (Stamatov et al., 2006) used pyrolysis oil for heating in boilers, furnaces, and kiln and reported that during combustion brighter, shorter and wider flames were observed in case of pyrolysis oil as compared to diesel fuel.

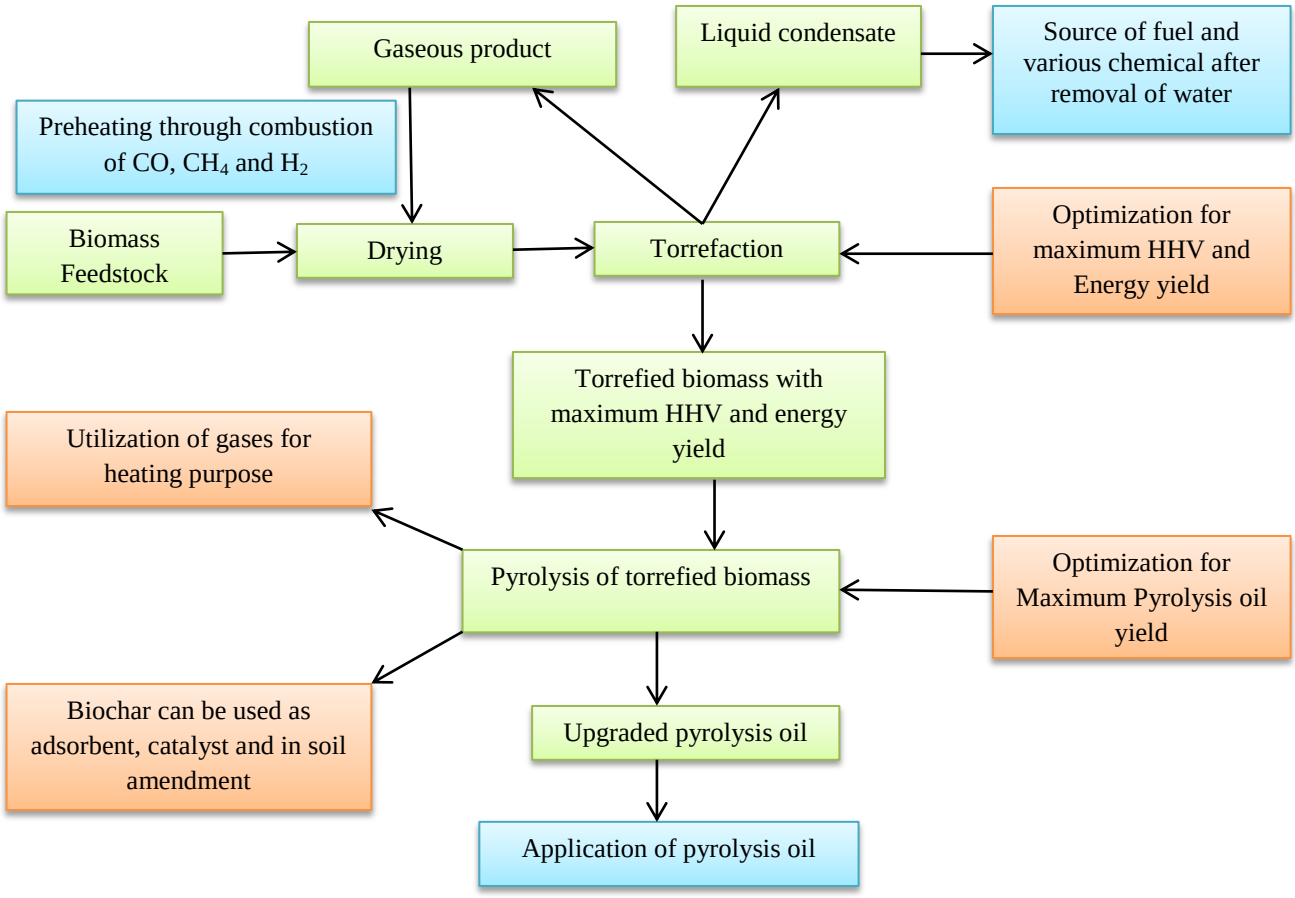

Figure 6.11 Proposed way to increase the sustainability of integrated torrefaction-pyrolysis process

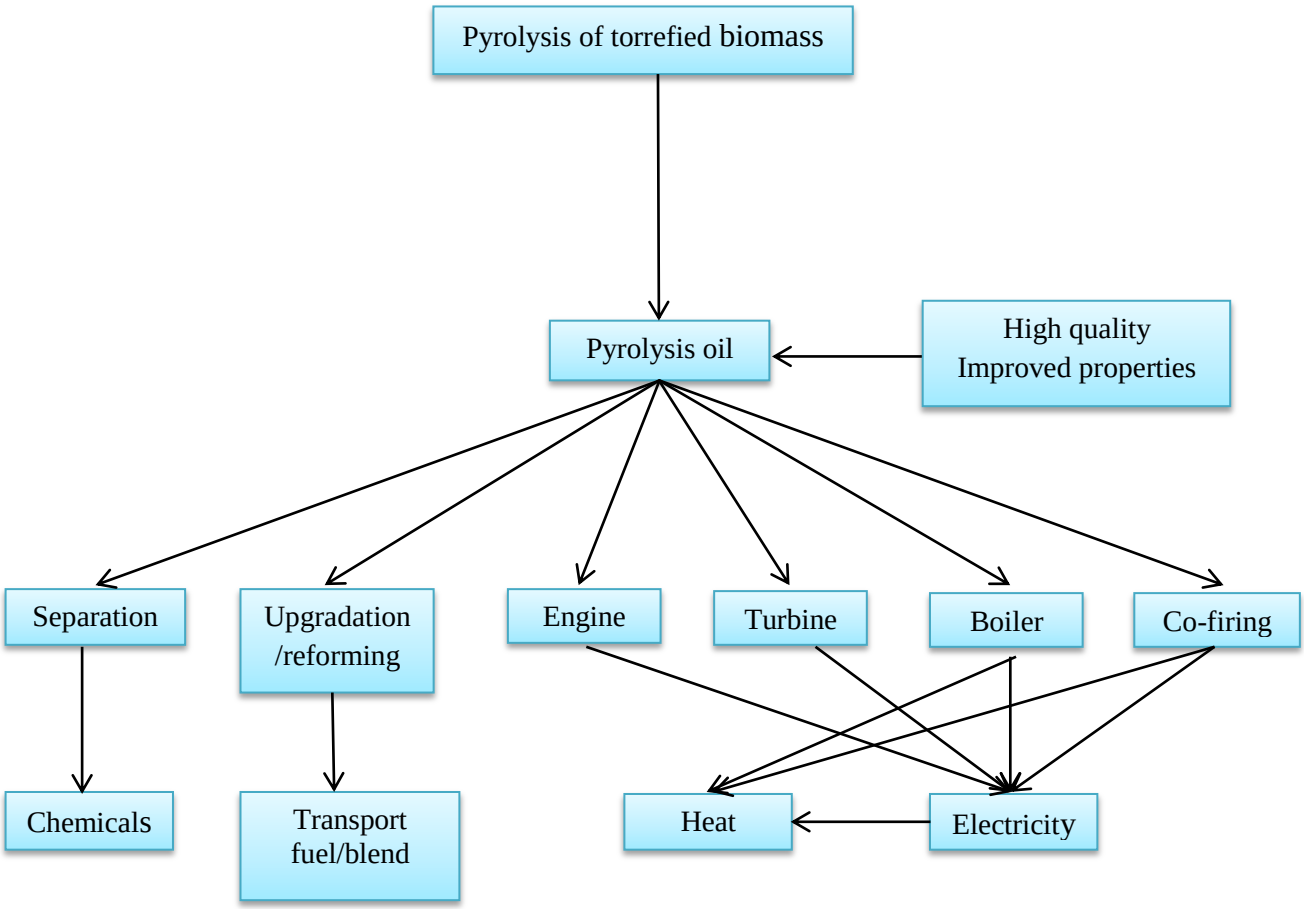

Figure 6.12 Possible applications of pyrolysis oil from pyrolysis of TAN-252-60-5 (adapted from references (Bridgwater, 2012; Dhyani & Bhaskar, 2018))

The biochar obtained from pyrolysis can be used in carbon sequestration, as an adsorbent in wastewater treatment, soil amendment,and as fuel (Dhyani & Bhaskar, 2018). The non-condensable gases produced may be used for external heating in other processes and recycling of gases into the pyrolytic reactor may enhance the heat integration as well as quality of pyrolysis oil (Mante et al., 2012). Besides, pyrolysis oil can be a good source of various chemical for industrial applications such as phenol and phenol derivatives such as

methylphenols, methoxyphenols can be used in resin, food, paints and pharmaceutical industries (Stoikos, 1991), organic acids can be used for the synthesis of levoglucosan, de-icers, hydroxyacetaldehydes and other additives which can be used in fiber manufacturing, fertilizer and pharmaceutical industries (Bogner et al., 2008; Dhyani & Bhaskar, 2018). The aldehydes present in pyrolysis oil can be used as a browning agents for meat, fish, poultry, cheese, and sausages (Ingemarsson et al., 1998). In all these applications, the efficacy of pyrolysis oil from TAN-252-60-5 may be better as compared to pyrolysis oil obtained from DAN.

6.4 Conclusions

Torrefaction improves many properties associated with DAN, while production of solid biofuels is the prime concern. Hence, pyrolysis of TAN-252-60-5 was carried out to obtain high-quality pyrolysis oil. A response surface methodology coupled with central composite design was employed to optimize the process using temperature, retention time and heating rate, and sweeping gas flow rate as independent variables. The main objective was to maximize the yield of pyrolysis oil. To compare the physicochemical characteristics of pyrolysis oil, the DAN was also pyrolysed at the optimum condition, e.g., temperature = 507.04 ℃, retention time = 58.25 min, heating rate = 38.00 ℃/min, sweeping gas flow rate = 40.52 mL/min. It was observed that pyrolysis oil obtained from TAN-252-60-5 was superior in terms of improved HHV, pH, and chemical composition and lower water content, etc. Also, optimization of two processes (torrefaction and pyrolysis) may further facilitate design, scale-up, and simulation of process reactor system. The pyrolysis oil obtained from pyrolysis of TAN-252-60-5 may be used effectively for direct heating in boilers and furnaces or as a blend in fossil-derived fuels. Also, many value-added

chemicals such as phenol and furfural derivatives may be extracted from pyrolysis oil and may be used for manufacturing resin, polymer composites, etc., and as adhesives in cement manufacturing.

Furthermore, to increase the sustainability of integrated process, the energy supplied during the torrefaction process may be offset by utilizing the enthalpy of gaseous products from torrefaction in heat recovery, and liquid products may be utilized as fuel or source of chemical after removal of water. The application of suitable catalysts in pyrolysis of TAN-252-60-5 may further increase the quality of pyrolysis oil and may mitigate the challenges of increased carbon residue and viscosity of pyrolysis oil obtained from TAN-252-60-5.

Thus, it may be concluded that combination of torrefaction with pyrolysis may increase the competitiveness of pyrolysis oil at a commercial scale due to its enhanced quality and improve overall sustainability in the biorefinery process, and also ensure waste minimization.